Bubble-raft model for a paraboloidal crystal

Mark J. Bowick, Luca Giomi, Homin Shin, and Creighton K. Thomas

Department of Physics, Syracuse University, Syracuse New York, 13244-1130

We investigate crystalline order on a two-dimensional paraboloid of revolution by assembling a single layer of millimeter-sized soap bubbles on the surface of a rotating liquid, thus extending the classic work of Bragg and Nye on planar soap bubble rafts. Topological constraints require crystalline configurations to contain a certain minimum number of topological defects such as disclinations or grain boundary scars whose structure is analyzed as a function of the aspect ratio of the paraboloid. We find the defect structure to agree with theoretical predictions and propose a mechanism for scar nucleation in the presence of large Gaussian curvature.

I. INTRODUCTION

Soft materials such as amphiphilic membranes, diblock copolymers, and colloidal emulsions can form ordered structures with a wide range of complex geometries and topologies. Macroscopic models of ordered systems of this type are desirable for direct visualization and table top demonstrations, and they can be used as control checks of theoretical predictions. In this paper, we discuss the fabrication of a paraboloidal soap bubble raft which realizes a two-dimensional crystalline monolayer with both variable Gaussian curvature and a boundary.

Some 60 years ago Bragg and Nye used bubble rafts to model metallic crystalline structures [1]. A carefully made assemblage of bubbles, floating on the surface of a soap solution and held together by capillary forces, forms an excellent two-dimensional replica of a crystalline solid, in which the regular triangular arrangement of bubbles is analogous to the close packed structure of atoms in a metal [2]. Feynman considered this technique to be important enough that the famous Feynman lectures in physics include a reproduction of the original Bragg-Nye paper in its entirety [3]. Bubble rafts can be made easily and inexpensively, equilibrate quickly, exhibit topological defects such as disclinations, dislocations and grain boundaries, and provide vivid images of the structure of defects. Bubble raft models have been used to study two-dimensional polycrystalline and amorphous arrays [4], nanoindentation of an initially defect-free crystal [5], and the dynamic behavior of crystals under shear [6]. Beyond these advantages, rotating the soap solution with bubbles on the surface provides a flexible playground for creating crystalline order on a nearly perfect paraboloid. Our emphasis here is to exhibit a macroscopic example of a curved crystal with an experiment simple enough to be suitable also for lecture demonstrations. This is a complement to, for example, mesoscale colloidal crystals formed at liquid-liquid emulsions and stabilized in a spherical geometry by surface tension [7,8]. Mesoscale curved crystals may be imaged by conventional optical or confocal microscopy but are more elaborate to prepare.

The interplay between order and geometry has been intensively studied in many systems, including large spherical crystals [9], toroidal hexatics [10], both crystals and hexatics draped over a Gaussian bump [11,12], and paraboloidal crystals [13]. Topological defects are essential in understanding the crystalline order in a curved two-dimensional manifold. In some cases (e.g., the sphere) the topology requires that a certain minimum number of defects be present in the ground state. For a two-dimensional Riemannian manifold M with boundary ∂M, a discrete version of the Gauss-Bonnet theorem for any triangulation of M reads

$$Q = \sum_{i \in M} (6 - c_i) + \sum_{i \in \partial M} (4 - c_i) = 6\chi, \tag{1}$$

where c_i is the coordination number of vertex i and χ is the Euler characteristic. The quantity $q_{i,M} = 6 - c_i$ is the disclination charge for a site i in the interior and measures the departure from perfect triangular order. The analogous quantity on the boundary is $q_{i,\partial M} = 4 - c_i$. Q thus represents the total disclination charge. For crystals on the two-sphere ($\chi = 2$), $Q = 12$, while for crystals on the two-torus ($\chi = 0$), $Q = 0$. For the disk topology relevant for our experiment, $\chi = 1$ and the total disclination charge $Q = 6$. Provided we restrict ourselves to the energetically preferred minimal $q = \pm 1$ disclinations, we see that any paraboloidal crystal must have at least six +1 disclinations [14].

In the regime of a sufficiently large number of particles, the isolated disclinations required by the topology are unstable to grain boundary "scars," consisting of arrays of tightly bound 5−7 pairs radiating from an unpaired +1 disclination. The existence of scars, first predicted in the context of spherical crystallography [9] and later observed experimentally in colloidal suspensions on spherical droplets [7,8], has become one of the fundamental signatures of dense geometrically frustrated systems. The possibility of a coexistence of isolated defects and scars was also pointed out [13] as a consequence of a variable Gaussian curvature in both frustrated and unfrustrated systems.

Calling z the height of the surface above the xy plane, a paraboloid is straightforwardly parametrized by the function $z(r) = \frac{h}{R^2}r^2$, where r is the polar distance on the xy plane, h the height of the paraboloid, and R the maximum radius. In order to provide a position-independent notion of curvature, it is convenient to introduce the parameter $\kappa = 2h/R^2$ representing the normal curvature of the paraboloid at the origin. A rotating fluid in a cylindrical vessel is a textbook example of a
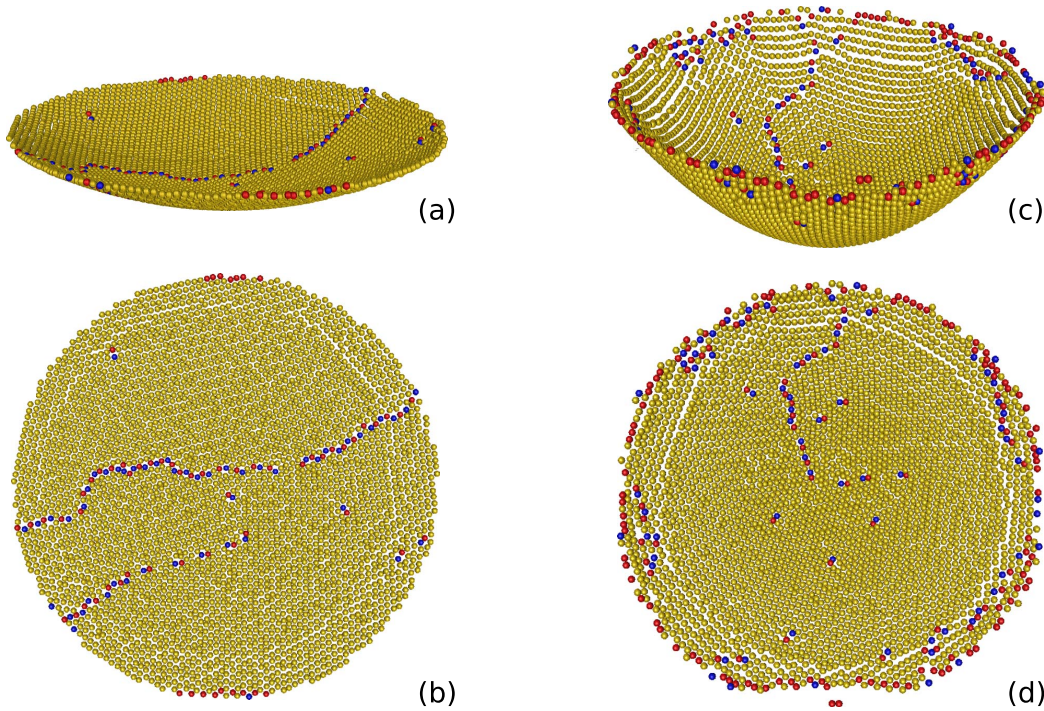
FIG. 1. (Color online) Lateral and top view of a computer reconstruction of two paraboloidal rafts with $\kappa_1 \approx 0.15$ cm^{-1} [(a), (b)] and $\kappa_2 \approx 0.32$ cm^{-1} [(c),(d)]. The number of bubbles is $N_1=3813$ and $N_2=3299$, respectively. The color scheme highlights the fivefold (red) and sevenfold (blue) disclinations over sixfold coordinated bubbles (yellow).

nearly perfect paraboloid of revolution. In this case $\kappa = \omega^2/g$, where ω is the angular velocity of the vessel and g the gravitational acceleration [15].

II. METHODS AND RESULTS

To make the bubble rafts, we pump air through a needle into soapy water. Because the larger bubble sizes we prefer are most easily made when the vessel is still, we first make the bubbles and only later spin the vessel to make the paraboloid (cf. Bragg and Nye [1], who spun their system in order to generate smaller bubbles but stopped the spinning to look at the bubbles on a flat surface). To image the bubbles, we mount a CCD digital camera on the top of the vessel, with lighting from a ring around the (clear) vessel to eliminate glare. The camera rotates along with the whole system so that the shutter speed is unimportant in imaging the bubbles. We use a second camera to find the aspect ratio of the paraboloid. We equilibrate the system and eliminate stacking of bubbles by imposing small perturbations of the angular frequency to mimic the role of thermal noise. The vessel has radius $R=5$ cm; the height of paraboloids varies from $h=0-4$ cm. The bubble diameter, extracted from the Delaunay triangulation of our images, is $a=0.84(1)$ mm with monodispersity $\Delta a/a \approx 0.003$. The normal curvature κ of the paraboloid at the origin varies from $0-0.32$ cm^{-1}. In addition to the flat disk, we observe two different curvature regimes: small curvature $\kappa_1 \approx 0.15$ cm^{-1} and large curvature $\kappa_2 \approx 0.32$ cm^{-1}. In each curvature class we collected several data sets with qualitatively similar results. In this paper, we present two characteristic data sets to illustrate our results.

Figure 1 shows a computer reconstruction of two bubble rafts with $\kappa=\kappa_1$ and κ_2, respectively. We extract two-dimensional coordinates from the images with a brightness based particle location algorithm through via the popular data analysis language IDL [16]. Data sets are then processed to correct possible imprecisions and finally Delaunay triangulated. The adjacency list obtained from the Delaunay triangulation is then used to determine the valency and the
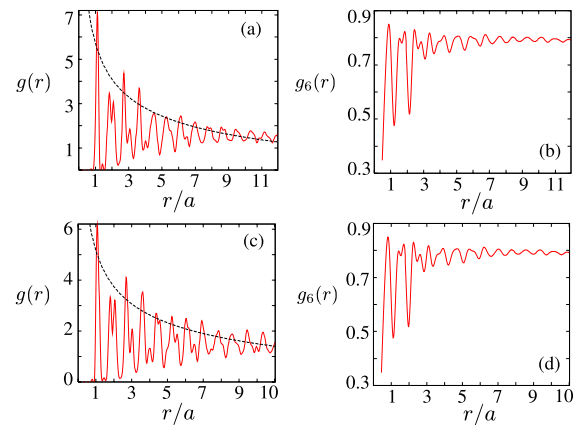

FIG. 2. (Color online) Translational and orientational correlation functions (g and g_6, respectively) for rafts with (a),(b) $\kappa \approx 0.32$ cm^{-1}, $a=(0.8410 \pm 0.0025)$ mm, and (c),(d) $\kappa \approx 0.15$ cm^{-1}, $a=(0.9071 \pm 0.0037)$ mm. All the curves are plotted as functions of r/a, where r is the planar distance from the center and a is the bubble radius. The envelope for the crystalline solid decays algebraically (dashed line), while the orientational correlation function approaches the constant value 0.8.

position of disclination defects. We choose to exclude from the triangulation the first $3-4$ bubble rings formed along the boundary of the cylindrical vessel, where the sharp concave meniscus due to the surface tension combined with the native curvature of the paraboloid was observed to produce a stacking of bubbles in a narrow double layer surrounding the perimeter of the vessel. This is the only significant boundary effect we observe in our system and does not hamper the identification of disclinations in the bulk.

To characterize the order of the crystalline raft, we measure the translational and orientational correlation functions $g(r)$ and $g_6(r)$ [17]. The former gives the probability of finding a particle at distance r from a second particle located at the origin. The function is normalized with the density of an equivalent homogeneous system in order to ensure $g(r)=1$ for a system with no structure. Interactions between particles build up correlations in their position and $g(r)$ exhibits decaying oscillations, asymptotically approaching one. For a two-dimensional solid with a triangular lattice structure the radial correlation function is expected to exhibit sharp peaks in correspondence with the sequence $r/a=\sqrt{n^2+nm+m^2}$ $=1,\sqrt{3},2,2\sqrt{3},\dots$, while the amplitude of the peaks decays algebraically as $r^{-\eta}$ with $\eta=1/3$ (dashed line in Fig. 2). Within the precision of our data, the positional order of the paraboloidal crystals assembled with the bubble raft model reflects this behavior, although with more accurate measurements, one might see dependence of the exponent η on the curvature (because of the proliferation of defects with curvature).

The orientational correlation function $g_6(r)$ is calculated as the average of the product $\langle\psi(0)\psi^*(r)\rangle$ of the hexatic order parameter over the whole sample. For each bubble (labeled j) that has two or more neighbors, $\psi_j(r)=(1/Z_j)\Sigma_{k=1}^{Z_j}\exp(6i\theta_{jk})$, where Z_j is the number neighbors of i and θ_{jk} is the angle between the j-k bonds and a reference axis. One expects $g_6(r)$ to decay exponentially in a disordered phase, algebraically in a hexatic phase and to approach a nonzero value in the case of a crystalline solid. In the systems studied we find that $g_6(r)$ to approaches value 0.8 in the distance of $5-6$ lattice spacings.

Of particular interest is the structure of the grain boundaries appearing in the paraboloidal lattice for different values of the curvature parameter κ. Grain boundaries form in the bubble array during the growing process as a consequence of geometrical frustration. As noted, any triangular lattice confined in a simply connected region with the topology of the disk is required to have a net disclination charge $Q=6$. Each disclination has an energy associated with long-range elastic distortion of the lattice and a short-range core energy. While the former is responsible for the emergent symmetry of a geometrically frustrated crystal, the latter plays the role of the energy penalty required for the creation of a single disclination defect. Although dependent on the interparticle interactions, and so different from system to system, the disclination core energy is generally much smaller than the elastic energy, especially in the case of a bubble array where the particle-particle interaction is dominated by hard-core repulsion. Defects are then favored to proliferate throughout the crystal. In the flat plane, however, the elastic stress due to
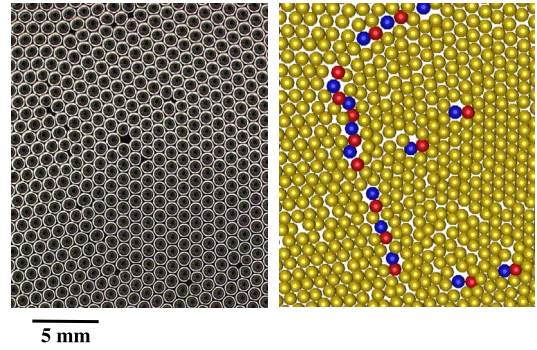

5 mm

FIG. 3. (Color online) An enlarged view of the terminating grain boundary scar shown in Fig. 1(d) for a system with large Gaussian curvature. The scar starts from the circular perimeter of the vessel and terminates roughly in the center carrying a net +1 topological charge. The image of the bubbles (left) shows that they may deform slightly to better fill space, whereas the computer reconstruction of the lattice (right) uses perfect spheres of uniform size.

an isolated disclination is extremely high and defects are energetically favored to cluster in the form of a grain boundary consisting of one-dimensional arrays of tightly bound $(5,7)$-fold disclinations pairs. In a planar confined system, grain boundaries typically span the entire length of the crystal, but if a nonzero Gaussian curvature is added to the medium, they can appear in the form of scars carrying a net +1 topological charge and terminating in the bulk of the crystal.

Prominent examples of grain boundaries are visible in the two lattices shown in Fig. 1. For a gently curved paraboloid (with $\kappa\approx0.15$ cm^{-1}), grain boundaries form long (possibly branched) chains running from one side to the other and passing through the center. As the curvature of the paraboloid is increased, however, this long grain boundary is observed to terminate in the center [see Fig. 1(d); a close-up version of this image is seen in Fig. 3]. For $R=5$ cm, the elastic theory of defects predicts a structural transition at $\kappa_c=0.27$ cm^{-1} in the limit of large core energies. In this limit the creation of defects is strongly penalized and the lattice has the minimum number of disclinations required by the topology of the embedding surface. In a low curvature paraboloid ($\kappa<\kappa_c$) these disclinations are preferentially located along the boundary to reduce the elastic energy of the system. When the aspect ratio of the paraboloid exceeds a critical value $\kappa_c(R)$, however, the curvature at the origin is enough to support the existence of a fivefold disclination and the system undergoes a structural transition. In the limit of large core energies, when only six disclinations are present, such a transition implies a change from the C_{6v} to the C_{5v} rotational symmetry group. A semiquantitative understanding of this phenomenon can be achieved by requiring the topological charge of a disclination located at the origin of the paraboloid to be exactly canceled by the smeared out Gaussian "curvature charge"

$$q_K=\int_0^{2\pi}d\phi\int_0^R dr\sqrt{g}K(r)=2\pi\left(1-\frac{1}{\sqrt{1+\kappa^2R^2}}\right),$$

where we have used $\sqrt{g}=r\sqrt{1+\kappa^2r^2}$ and $K=\kappa^2/(1+\kappa^2r^2)^2$. Upon equating q_K to $2\pi/6$, the charge of a single disclination, one finds

$$\kappa_c(R) \approx \frac{\sqrt{11}}{5R}. \tag{2}$$

Therefore, when $\kappa > \kappa_c(R)$, the Gaussian curvature of the paraboloid is sufficient to balance the elastic stress introduced by the central disclination and the bulk of the system acquires a net positive disclination charge. This simple argument neglects disclination core energies as well as the actual elastic interaction between defects and curvature. A rigorous treatment can be found in Ref. [13].

Together with our experimental observations, these considerations point to the following mechanism for scar nucleation in a paraboloidal crystal. In the regime in which the creation of defects is energetically inexpensive, geometrical frustration due to the confinement of the lattice in a simply connected region is responsible for the formation of a long side-to-side grain boundary. However, when the curvature of the paraboloid exceeds a critical value (dependent on the radius of the circular boundary), the existence of a +1 disclination near the center is energetically favored. Such a disclination serves as a nucleation site for $5-7$ dislocations and the side-to-side grain boundary is replaced by a terminating center-to-side scar. Above the critical curvature the theory also predicts a regime of coexistence of isolated disclinations and scars due to the variable Gaussian curvature. For dense systems (i.e., number of subunits larger than a few hundred for our geometry), the coexistence is suppressed because the embedding surface will appear nearly flat at the length scale of a lattice spacing. The bulk of the system is thus populated uniquely by scars. This is consistent with our experimental observation.

Away from the center of the paraboloid, we have compared the crystalline directions with the geodesics starting from a given reference point (see Fig. 4). Near the boundary, the directions of both first and second neighbors (in red and blue, respectively), are reasonably aligned with the geodesics. The alignment becomes decorrelated after roughly five lattice spacings with the decorrelation more pronounced in the radial direction (maximal principal curvature) where the normal curvature is largest. As one gets closer to the center, the geodesic correlation becomes weaker and almost completely vanishes along the radial direction. Along the angular direction (minimal principal curvature), on the other hand, the crystalline axes appear aligned with the geodesic directions.

III. CONCLUSIONS

In this paper we have discussed the experimental preparation of a paraboloidal crystal which is readily visualized. Despite the simplicity of our technique we found good agreement with the elastic theory of defects in curved space. Bubble rafts are shown to be effective models for the study of curved crystallography. Bubble assemblages provide a large number of particles (order 10^3) with very simple and inexpensive equipment. They give access to details that are
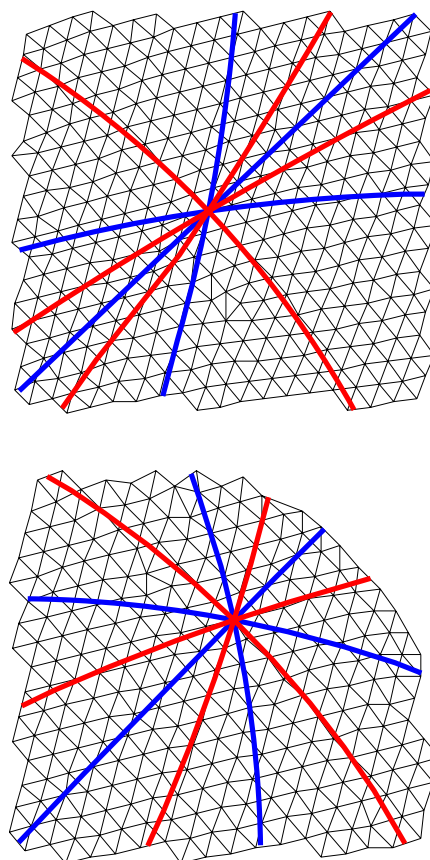

FIG. 4. (Color online) Delaunay triangulation of a portion of the paraboloidal lattice with $\kappa \approx 0.32$ cm^{-1} near the center (top) and the boundary (bottom). Red (lighter) and blue (darker) lines represent the geodesics directed toward first and second neighbors, respectively.

necessarily unavailable to continuous field theories and provide system sizes that are prohibitive for numerical simulations.

Future experiments might explore varying the shape of the vessel to investigate the role of the boundary on the bulk order. This setup is also suitable for studying dynamical phenomena such as the glide of dislocations in the relaxation process as well as the formation of vacancies and interstitials (e.g., following Ritacco *et al.* [18], looking at a cascade of bursting bubbles on a paraboloid).

[1] W. L. Bragg and J. F. Nye, Proc. R. Soc. London, Ser. A **190**, 474 (1947).

[2] C. Kittel, *Introduction to Solid State Physics* (Wiley, New York, 1966).

[3] R. P. Feynman, R. B. Leighton, and M. Sands, *Feynman Lectures on Physics* (Addison-Wesley, Reading, MA, 1963), Vol. 2, Chap. 30.

[4] A. W. Simpson and P. H. Hodkinson, Nature (London) **237**, 320 (1972).

[5] A. Gouldstone, K. J. Van Vliet, and S. Suresh, Nature (London) **411**, 656 (2001).

[6] Y. Wang, K. Krishan, and M. Dennin, Phys. Rev. E **73**, 031401 (2006).

[7] A. R. Bausch, M. J. Bowick, A. Cacciuto, A. D. Dinsmore, M. F. Hsu, D. R. Nelson, M. G. Nikolaides, A. Travesset, and D. A. Weitz, Science **299**, 1716 (2003).

[8] P. Lipowsky, J. Schilling, M. J. Bowick, and A. Bausch, Langmuir **21**, 12076 (2005).

[9] M. J. Bowick, D. R. Nelson, and A. Travesset, Phys. Rev. B **62**, 8738 (2000); M. Bowick, A. Cacciuto, D. R. Nelson, and A. Travesset, Phys. Rev. Lett. **89**, 185502 (2002); A. Perez-Garrido, M. J. W. Dodgson, and M. A. Moore, Phys. Rev. B **56**, 3640 (1997).

[10] M. Bowick, D. R. Nelson, and A. Travesset, Phys. Rev. E **69**, 041102 (2004).

[11] V. Vitelli and D. R. Nelson, Phys. Rev. E **70**, 051105 (2004).

[12] V. Vitelli, J. B. Lucks, and D. R. Nelson, Proc. Natl. Acad. Sci. U.S.A. **103**, 12323 (2006).

[13] L. Giomi and M. J. Bowick, Phys. Rev. B **76**, 054106 (2007).

[14] A. A. Koulakov and B. I. Shklovskii, Phys. Rev. B **57**, 2352 (1998); M. Kong, B. Partoens, A. Matulis, and F. M. Peeters, Phys. Rev. E **69**, 036412 (2004); A. Mughal and M. A. Moore, *ibid.* **76**, 011606 (2007).

[15] M.P. Spiegel *Applied Differential Equations* (Prentice-Hall, Englewood Cliffs, NJ, 1958), p 121.

[16] J. C. Crocker and D. G. Grier, J. Colloid Interface Sci. **179**, 298 (1996).

[17] D. R. Nelson *Defects and Geometry in Condensed Matter Physics* (Cambridge University Press, Cambridge, 2000).

[18] H. Ritacco, F. Kiefer, and D. Langevin, Phys. Rev. Lett. **98**, 244501 (2007).